for integer frustrations. Notably, the observed value of $\varepsilon = {}^{2}/_{3}$ for the integer dynamic transition coincides with the corresponding mean-field value for the temperature- and pressure-driven thermodynamic electronic Mott transition (*21*) belonging in the class of the liquid-gas transition of classical systems (*1*, *21*, *22*). The universal scaling properties of the current- and magnetic field–dependent dynamical resistivity experimentally demonstrate that a vortex Mott insulator undergoes a phase transition resembling a liquid-to-gas transition at the nonequilibrium critical end point. The critical exponent at $f_c = {}^{1}/_{2}$ is $\varepsilon = {}^{1}/_{2}$, indicating that fractional vortex Mott transitions belong in different universality classes.

REFERENCES AND NOTES

1. L. P. Kadanoff *et al.*, *Rev. Mod. Phys.* **39**, 395–431 (1967).
2. M. E. Fisher, *Rev. Mod. Phys.* **46**, 597–616 (1974).
3. M. Henkel, H. Hinrichsen, S. Lübeck, *Non-Equilibrium Phase Transitions* (Springer, New York, 2008).
4. R. S. Newrock, C. J. Lobb, U. Geigenmüller, M. Octavio, *Solid State Phys.* **54**, 263–512 (1999).
5. D. R. Nelson, V. M. Vinokur, *Phys. Rev. B* **48**, 13060–13097 (1993).
6. M. Baert, V. V. Metlushko, R. Jonckheere, V. V. Moshchalkov, Y. Bruynseraede, *Phys. Rev. Lett.* **74**, 3269–3272 (1995).
7. K. Harada *et al.*, *Science* **274**, 1167–1170 (1996).
8. S. Goldberg *et al.*, *Phys. Rev. B* **79**, 064523 (2009).
9. See supplementary materials on *Science* Online.
10. M. Tinkham, D. W. Abraham, C. J. Lobb, *Phys. Rev. B* **28**, 6578–6581 (1983).
11. T. I. Baturina, Yu. A. Tsaplin, A. E. Plotnikov, M. R. Baklanov, *JETP Lett.* **81**, 10–14 (2005).
12. S. Eley, S. Gopalakrishnan, P. M. Goldbart, N. Mason, *Nat. Phys.* **8**, 59–62 (2012).
13. D. R. Hofstadter, *Phys. Rev. B* **14**, 2239–2249 (1976).
14. T. I. Baturina *et al.*, *Europhys. Lett.* **93**, 47002 (2011).
15. S. P. Benz, M. S. Rzchowski, M. Tinkham, C. J. Lobb, *Phys. Rev. B* **42**, 6165–6171 (1990).
16. Z. Jiang, D. A. Dikin, V. Chandrasekhar, V. V. Metlushko, V. V. Moshchalkov, *Appl. Phys. Lett.* **84**, 5371–5373 (2004).
17. M. J. Rozenberg, R. Chitra, G. Kotliar, *Phys. Rev. Lett.* **83**, 3498–3501 (1999).
18. G. Blatter, M. V. Feigel'man, V. B. Geshkenbein, A. I. Larkin, V. M. Vinokur, *Rev. Mod. Phys.* **66**, 1125–1388 (1994).
19. J. Kierfeld, H. Nordborg, V. M. Vinokur, *Phys. Rev. Lett.* **85**, 4948–4951 (2000).
20. L. D. Landau, E. M. Lifshitz, *Quantum Mechanics* (Elsevier, Oxford, 1977)
21. P. Limelette *et al.*, *Science* **302**, 89–92 (2003).
22. G. Kotliar, E. Lange, M. J. Rozenberg, *Phys. Rev. Lett.* **84**, 5180–5183 (2000).
23. P. G. Harper, *Proc. Phys. Soc. A* **68**, 874–878 (1955).

ACKNOWLEDGMENTS

We thank M. Lankhorst, F. Roesthuis, and D. Veldhuis for help during the experiments. Supported by the Dutch FOM and NWO foundations; the U.S. Department of Energy, Office of Science, Materials Sciences and Engineering Division; and Ministry of Education and Science of the Russian Federation grant 14.Y26.31.0007. N.P. and T.I.B. acknowledge for financial support the Marie Curie IEF and the Alexander von Humboldt Foundation, respectively. All data are available in the supplementary materials. Author contributions: N.P. conceived and designed the experiment; N.P., F.C., C.G.M., and X.R.W. performed the experiments; V.M.V. conceived the theoretical concept; T.I.B. and V.M.V. analyzed experimental data and developed a theory; A.A.G., A.B., G.B., and H.H. contributed to the theoretical description; and all authors contributed in writing the manuscript.

SUPPLEMENTARY MATERIALS

www.sciencemag.org/content/349/6253/1202/suppl/DC1
Materials and Methods
Supplementary Text
Figs. S1 and S2
Reference (*24*)

27 August 2014; accepted 29 July 2015
10.1126/science.1260507

QUANTUM MECHANICS

A self-interfering clock as a "which path" witness

Yair Margalit, Zhifan Zhou, Shimon Machluf,* Daniel Rohrlich, Yonathan Japha, Ron Folman†

In Einstein's general theory of relativity, time depends locally on gravity; in standard quantum theory, time is global—all clocks "tick" uniformly. We demonstrate a new tool for investigating time in the overlap of these two theories: a self-interfering clock, comprising two atomic spin states. We prepare the clock in a spatial superposition of quantum wave packets, which evolve coherently along two paths into a stable interference pattern. If we make the clock wave packets "tick" at different rates, to simulate a gravitational time lag, the clock time along each path yields "which path" information, degrading the pattern's visibility. In contrast, in standard interferometry, time cannot yield "which path" information. This proof-of-principle experiment may have implications for the study of time and general relativity and their impact on fundamental effects such as decoherence and the emergence of a classical world.

Two-slit interferometry of quanta, such as photons and electrons, figured prominently in the Bohr-Einstein debates on the consistency of quantum theory (*1*, *2*). A fundamental principle emerging from those debates—intimately related to the uncertainty principle—is that "which path" information about the quanta passing through slits blocks their interference. At the climax of the debates, Einstein claimed that a clock, emitting a photon at a precise time while being weighed on a spring scale to measure the change in its mass-energy, could evade the uncertainty principle. Yet Bohr showed that the clock's gravitational redshift induces enough uncertainty in the emission time to satisfy the uncertainty principle. Inspired by the subtle role that time may play, we have now sent a clock through a spatial interferometer. Our proof-of-principle experiment introduces clock interferometry as a new tool for studying the interplay of general relativity (*3*) and quantum mechanics (*4*).

Time in standard quantum mechanics is a global parameter, which cannot differ between paths. Hence, in standard interferometry (*5*) a difference in height between two paths merely affects their relative phase, shifting their interference pattern without degrading its visibility. In contrast, general relativity predicts that a clock must "tick" slower along the lower path; thus if the paths of a clock through an interferometer have different heights, a time differential between the paths will yield "which path" information and degrade the visibility of the interference pattern (*6*). Consequently, whereas standard interferometry may probe general relativity (*7*–*9*), clock interferometry probes the interplay of general relativity and quantum mechanics. For example, loss of visibility because of a proper time lag would be evidence that gravitational effects contribute to decoherence and the emergence of a classical world (*10*).

Although our interferometer is of a new type, it is worthwhile noting decades of progress in matter-wave interferometry (*11*). Specifically, we note experiments in which neutron spins have been rotated in a magnetic field (*12*, *13*) and experiments in which different paths were labeled (*14*). For completeness, we also note recent work on the so-called Compton clock interferometer (*15*) and the debates that ensued [(*16*, *17*) and references therein].

In our experiment, atomic clocks—atoms in superpositions of internal states—pass through an atomic matter-wave interferometer. We demonstrate that the visibility of interference patterns produced by thousands of self-interfering clocks [atoms in a Bose-Einstein condensate (BEC)] depends on the (simulated) proper time differential between the recombined wave packets of each clock. We simulated the time differential or lag by artificially making one clock wave packet "tick" faster than the other. Although our clock is not accurate enough to be sensitive to special- or general-relativistic effects, it is able to demonstrate that a differential time reading affects the visibility of a clock self-interference pattern (*6*); specifically, the visibility equals the scalar product of the interfering clock states.

In principle, any system evolving with a well-defined period can be a clock. We used a quantum two-level system: a ^{87}Rb atom in a superposition of two Zeeman sublevels, the $m_F = 1$ and $m_F = 2$ sublevels of the $F = 2$ hyperfine state.

The general scheme of the clock interferometer is shown in Fig. 1 (*18*). To prepare the clock in a superposition of two different locations, we made use of the previously demonstrated Stern-Gerlach type matter-wave interferometer on an atom chip (*19*), creating a coherent spatial superposition of a ^{87}Rb BEC (~10^4 atoms) 90 μm below the chip surface. Initially, after the application of a field gradient beam splitter (FGBS) and a stopping pulse that zeroes the relative velocity of

Department of Physics, Ben-Gurion University of the Negev, Beer-Sheva 84105, Israel.
*Present address: Van der Waals-Zeeman Institute, University of Amsterdam, Science Park 904, 1090 GL Amsterdam, Netherlands.
†Corresponding author. E-mail: folman@bgu.ac.il

the two atomic wave packets, the wave packets are in the same internal atomic state ($|F, m_F\rangle = |2, 2\rangle \equiv |2\rangle$) as well as in the same external momentum state. A radio-frequency (RF) $\pi/2$ pulse (Rabi frequency Ω_R and duration T_R) tuned to the transition from $|2\rangle$ to $|1\rangle \equiv |2, 1\rangle$ forms the clock by transferring the atoms from the $|2\rangle$ state to the internal superposition state $(|1\rangle + |2\rangle)/\sqrt{2}$.

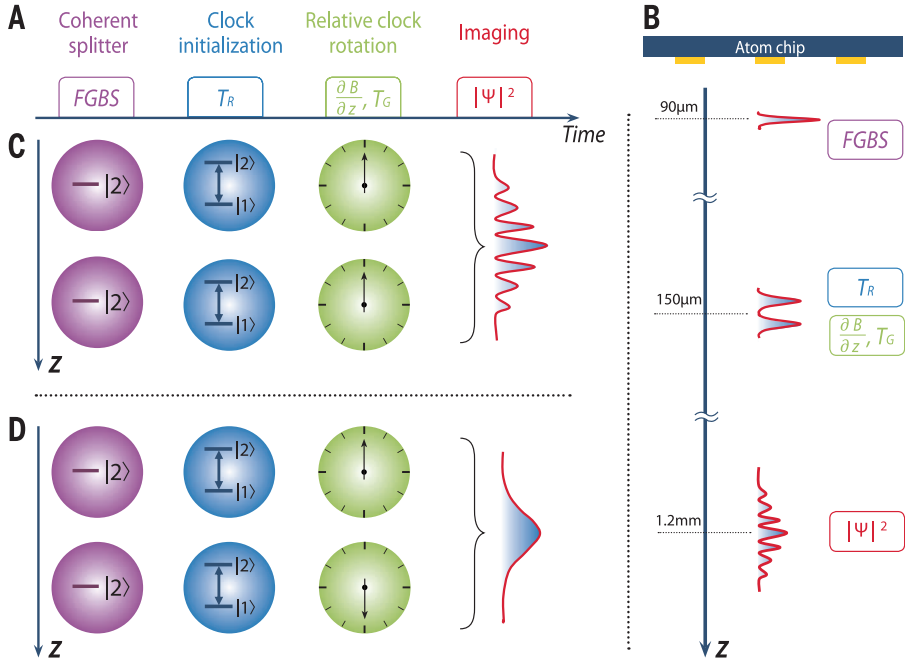

Fig. 1. Experimental sequence of the clock interferometer. (**A**) Detailed sequence (not to scale). After a coherent spatial splitting by the FGBS and a stopping pulse, the system consists of two wave packets in the $|2\rangle$ state (separated along the *z* axis, the direction of gravity) with zero relative velocity (*19*). The clock is then initialized with a RF pulse of length T_R, after which the relative "tick" rate of the two clock wave packets may be changed by applying a magnetic field gradient $\partial B/\partial z$ of duration T_G. Last, before an image is taken (in the *xz* plane) the wave packets are allowed to expand and overlap. (**B**) The same sequence as in (A) presented in space (in the *yz* plane). The chip wires are parallel to *x*, and the imaging beam is parallel to *y*. (**C**) Evolution in time, synchronized with (A). Each clock wave packet shows as a one-handed clock, in which the hand corresponds to a vector in the equatorial plane of the Bloch sphere. When the clock reading (the position of the clock hand) in the two clock wave packets is the same, fringe visibility is high. (**D**) When the clock reading is opposite (orthogonal), it becomes a "which path" witness, and there is no interference pattern.

The pulse is applied under a strong homogeneous magnetic field in order to push the transition to $|2, 0\rangle$ out of resonance via the nonlinear Zeeman effect, thus forming a pure two-level system (*18*).

In order to examine the coherence of the clock spatial superposition, we let the two clock wave packets freely expand and overlap to create spatial interference fringes (Fig. 2A). Because two BEC wave packets are always expected to yield fringes when they overlap, many experimental cycles are required in order to prove phase stability or, in other words, coherent splitting of the clock. In the averaged picture of 100 single shots taken continuously over a period of ~2 hours (Fig. 2B), the contrast falls by a mere 2% relative to the mean of the single-shot visibility, demonstrating a stable phase. The narrow phase distribution in the data (*18*) reveals that the clock splitting is coherent (meaning the clock was in a superposition of two locations).

We now show that clock time is indeed a "which path" witness. For a single-internal-state interferometer, a phase difference will not change the visibility of the fringes. In contrast, the relative rotation between the two clock wave packets is expected to influence the interferometric visibility. In the extreme case, when the two clock states are orthogonal—for example, one in the state $(|1\rangle + |2\rangle)/\sqrt{2}$ and the other in the state $(|1\rangle - |2\rangle)/\sqrt{2}$—the visibility of the clock self-interference should drop to zero. We applied a magnetic gradient pulse [inducing a "tick" rate difference $\Delta\omega$ (*18*)] of duration T_G so as to induce a relative angle of rotation between the two clock wave packets (Fig. 1). When the relative rotation angle is π, we observed in a single shot that the visibility of the interference pattern drops to zero (Fig. 2C). Again, this is unlike standard interferometers in which a phase difference does not suppress visibility, which this is contrary to standard split-BEC interference experiments in

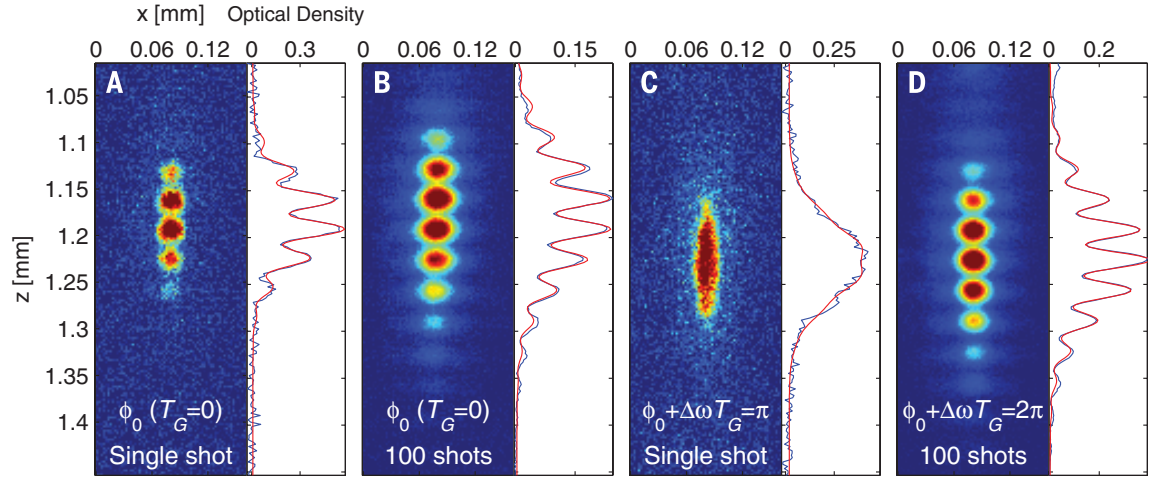

Fig. 2. Clock interference. (**A**) A single experimental shot of a clock interfering with itself (*z* axis values are relative to the chip surface). As $T_G = 0$, the clock rate is approximately the same in the two wave packets, and interference is visible. As can be seen from Fig. 3, a constant differential rotation of the clocks, ϕ_0, exists even for $T_G = 0$ [because of a residual magnetic gradient in our chamber (*18*)]. This somewhat reduces the visibility. (**B**) To prove the coherence of the clock spatial splitting, an average of 100 consecutive shots such as that in (A) is presented, with only a 2% drop in visibility (*18*). (**C**) To prove that clock time acts as a "which path" witness, we present a single shot in which the differential rotation angle $\phi_0 + \Delta\omega T_G$ equals π. (**D**) Similar to (B), but where indistinguishability is restored by $\phi_0 + \Delta\omega T_G = 2\pi$ (visibility is 47 ± 1%, down from a single-shot average of 51 ± 2%). The fits are a simple combination of a sine with a Gaussian envelope (*19*). The vertical position as well as the vertical extent of the clouds is explained in (*18*). Throughout this work, all data samples are from consecutive measurements without any post-selection or post-correction.

which a single shot always exhibits substantial visibility. A revival of the single-shot visibility is seen when the differential rotation angle is taken to be 2π (where we again present an average of 100 shots to confirm coherence) (Fig. 2D).

To obtain a more general view of the effect, we studied the dependence of the interference pattern visibility on the differential rotation angle between the two clock wave packets over the range 0 to 4π, by varying T_G to alternate between clock indistinguishability and orthogonality (Fig. 3). The blue data in Fig. 3 present the clock interference pattern visibility, clearly showing oscillations [consistent with the expected period (*18*)]. Comparing the latter oscillations with the visibility of a single-internal-state "no clock" interference ($\Omega_R T_R = 0$) (Fig. 3, red data) confirms that the oscillations are due to the existence of a clock. The single-internal-state interference data also confirm that the overall drop in visibility is not due to the formation of the clock. This upper bound is due to the magnetic gradient pulse causing imperfect overlap between the two wave packets (*18*). A lower bound on the visibility is due to the spatial separation of the $|1\rangle$ and $|2\rangle$ wave packets (gradual breakup of the clock), again due to the magnetic gradient (*18*), which results in an increase of the visibility as expected from two independent single-state interferometers.

The essence of the clock is that it consists of a superposition of two levels, $|1\rangle$ and $|2\rangle$. In Fig. 3, we chose to work with an equal population of the $|1\rangle$ and $|2\rangle$ states upon clock initialization to create a proper clock, thus maximizing the visibility's dependence on the differential rotation. To further prove that it is the clock reading that is responsible for the observed oscillations of visibility, we modulated the very formation of the clock by varying the clock-initiating RF pulse (T_R) so that the system preparation alternates between a proper clock and no clock at all (Fig. 4). Specifically, varying T_R changes the population ratio of the two components of the clock. When the differential rotation of the two clock wave packets ($\Delta\omega T_G$) is set to π (orthogonal clocks), as shown by the blue data in Fig. 4A, the interferometer visibility oscillates as a function of the ratio of the clock states' initial population. This is so because when $\Omega_R T_R$ equals multiples of π, only one of the clock states is populated, and the system is actually not a clock. In this case, we have a standard interferometer; "clock orthogonality" and clock time as a "which path" witness do not exist irrespective of the fact that $\Delta\omega T_G = \pi$, and consequently, full visibility is obtained. When a proper clock is formed (equal initial populations), clock time is an effective witness, and the visibility drops. In contrast, when $\Delta\omega T_G = 2\pi$ (Fig. 4A, red data), the interferometer visibility is always high because the two wave packets are not orthogonal whether they are clocks or states with a definite m_F.

Our realization of clock interferometry demonstrates a way to probe the interplay between quantum mechanics and general relativity. In this context, some even suggest that wave-function collapse may be due to gravity (*20*–*22*). It remains to be seen whether clock interferometers can provide new insight regarding such mechanisms as well. In addition, because time is considered by some a parameter that is still far from being fully understood (*23*), such an interferometer may shed new light on a variety of related fundamental questions.

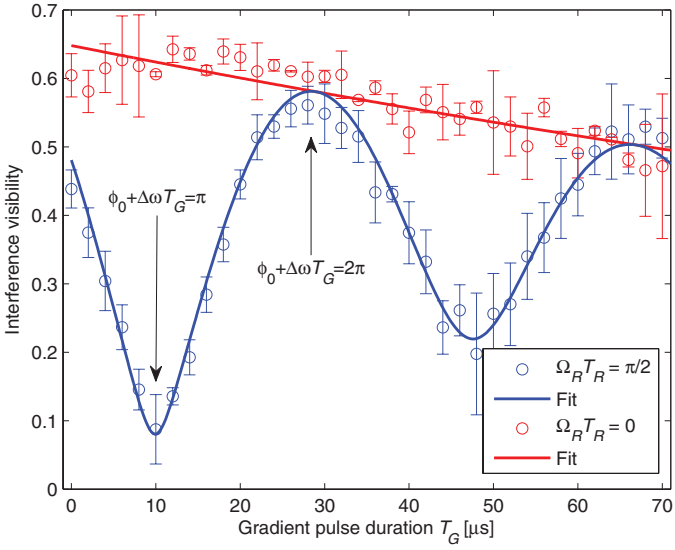

Fig. 3. Varying the orthogonality of the two clock wave packets. To study the properties of clock time as a "which path" witness, we measure visibility while continuously varying the relative rotation of the two clock wave packets (blue). Each data point is an average of the single-shot visibility obtained in several experimental cycles, and the error bars are the variance in this subsample. A fit returns an oscillation constant of $\Delta\omega = 0.166 \pm 0.003$ rad/μs, which is consistent with an independent estimate (*18*). As inferred from the single-internal-state "no clock" interferometer (red line), the oscillations are due to the existence of a clock. The upper and lower bounds are explained in the text.

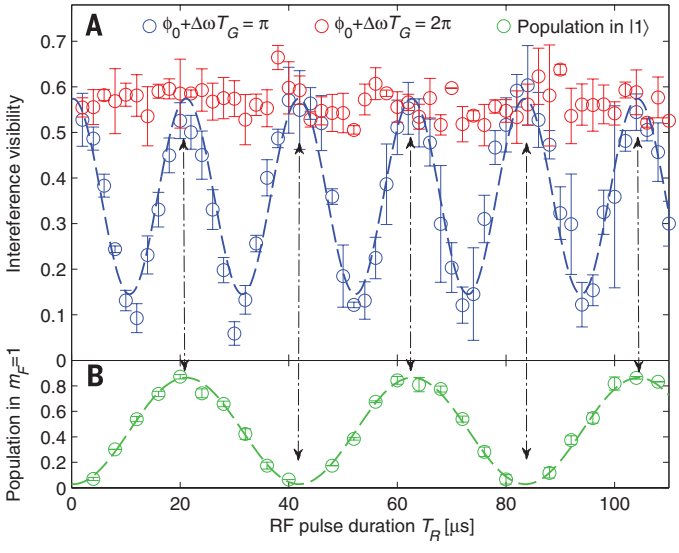

Fig. 4. Varying the preparation of the clock. To further prove that it is the clock reading that is responsible for the observed oscillations in visibility, we modulate the very formation of the clock by varying T_R, so that the system preparation alternates between a proper clock and no clock at all. (**A**) When the imprinted relative rotation between the two clock wave packets is π, whether a proper clock is formed or not has a dramatic effect (blue). In contrast, when the relative rotation is 2π, whether a proper clock is formed or not has no effect (red). The error bars are the standard deviation of several data points. (**B**) The oscillation period appearing in (A) is as expected from an independent measurement of the Rabi oscillations induced by T_R when the rest of the RF sequence has been eliminated (*18*).

REFERENCES AND NOTES

1. N. Bohr, in *Albert Einstein: Philosopher–Scientist*, P. A. Schilpp, Ed. (Tudor, New York, 1951), pp. 201–41.
2. Y. Aharonov, D. Rohrlich, *Quantum Paradoxes: Quantum Theory for the Perplexed* (Wiley-VCH, Weinheim, Germany, 2005), section 2.4.
3. M. Moerchen, R. Coontz, *Science* **347**, 1083 (2015).
4. I. Georgescu, *Nat. Phys.* **10**, 253 (2014).
5. R. Colella, A. W. Overhauser, S. A. Werner, *Phys. Rev. Lett.* **34**, 1472–1474 (1975).
6. M. Zych, F. Costa, I. Pikovski, Č. Brukner, *Nat. Commun.* **2**, 505 (2011).
7. S. Dimopoulos, P. W. Graham, J. M. Hogan, M. A. Kasevich, *Phys. Rev. Lett.* **98**, 111102 (2007).
8. H. Müntinga *et al.*, *Phys. Rev. Lett.* **110**, 093602 (2013).
9. C. C. N. Kuhn *et al.*, *New J. Phys.* **16**, 073035 (2014).
10. I. Pikovski, M. Zych, F. Costa, Č. Brukner, *Nat. Phys.* (2015).
11. A. D. Cronin, J. Schmiedmayer, D. E. Pritchard, *Rev. Mod. Phys.* **81**, 1051–1129 (2009).
12. H. Rauch *et al.*, *Phys. Lett. A* **54**, 425–427 (1975).

13. H. Rauch, S. A. Werner, *Neutron Interferometry: Lessons in Experimental Quantum Mechanics* (Calderon Press, Oxford, UK, 2000).
14. S. Dürr, T. Nonn, G. Rempe, *Nature* **395**, 33–37 (1998).
15. S.-Y. Lan *et al.*, *Science* **339**, 554–557 (2013).
16. W. P. Schleich, D. M. Greenberger, E. M. Rasel, *Phys. Rev. Lett.* **110**, 010401 (2013).
17. S. Peil, C. R. Ekstrom, *Phys. Rev. A* **89**, 014101 (2014).
18. Materials and methods are available as supplementary materials on *Science* Online.
19. S. Machluf, Y. Japha, R. Folman, *Nat. Commun.* **4**, 2424 (2013).
20. R. Penrose, *The Emperor's New Mind: Concerning Computers, Minds, and the Laws of Physics* (Oxford Univ. Press, New York, 1989), chap. 6.
21. L. Diósi, *J. Phys. Conf. Ser.* **442**, 012001 (2013).
22. A. Bassi, K. Lochan, S. Satin, T. P. Singh, H. Ulbricht, *Rev. Mod. Phys.* **85**, 471–527 (2013).
23. Lee Smolin, *Time Reborn* (Mariner Books, Wilmington, MA, 2014).

ACKNOWLEDGMENTS

We thank Z. Binshtok, S. Zhou, M. Keil, D. Groswasser, Y. Bar-Haim, and M. Givon for their assistance and the Ben-Gurion University of the Negev nanofabrication facility for providing the high-quality chip. This work is funded in part by the Israeli Science Foundation, the European Commission "MatterWave"' consortium (FP7-ICT-601180), and the German-Israeli DIP project (Quantum phenomena in hybrid systems) supported by the Deutsche Forschungsgemeinschaft. We also acknowledge support from the program for outstanding postdoctoral researchers of the Israeli Council for Higher Education and from the Ministry of Immigrant Absorption (Israel). D.R. thanks the John Templeton Foundation (Project ID 43297) and the Israel Science Foundation (grant 1190/13) for support. The opinions expressed in this publication do not necessarily reflect the views of the John Templeton Foundation.

SUPPLEMENTARY MATERIALS

www.sciencemag.org/content/349/6253/1205/suppl/DC1
Materials and Methods
Supplementary Text
Figs. S1 to S4
References (*24*–*28*)

27 May 2015; accepted 21 July 2015
Published online 6 August 2015
10.1126/science.aac6498

ELECTROCHEMISTRY

Covalent organic frameworks comprising cobalt porphyrins for catalytic CO_2 reduction in water

Song Lin,[1,2]* Christian S. Diercks,[1,3]* Yue-Biao Zhang,[1,3,4]* Nikolay Kornienko,[1] Eva M. Nichols,[1,2] Yingbo Zhao,[1] Aubrey R. Paris,[1] Dohyung Kim,[5] Peidong Yang,[1,3,5,6] Omar M. Yaghi,[1,3,6,7]† Christopher J. Chang[1,2,8,9]†

Conversion of carbon dioxide (CO_2) to carbon monoxide (CO) and other value-added carbon products is an important challenge for clean energy research. Here we report modular optimization of covalent organic frameworks (COFs), in which the building units are cobalt porphyrin catalysts linked by organic struts through imine bonds, to prepare a catalytic material for aqueous electrochemical reduction of CO_2 to CO. The catalysts exhibit high Faradaic efficiency (90%) and turnover numbers (up to 290,000, with initial turnover frequency of 9400 $hour^{-1}$) at pH 7 with an overpotential of −0.55 volts, equivalent to a 26-fold improvement in activity compared with the molecular cobalt complex, with no degradation over 24 hours. X-ray absorption data reveal the influence of the COF environment on the electronic structure of the catalytic cobalt centers.

Global energy demands and climate change underpin broad interest in the sustainable reductive transformation of carbon dioxide (CO_2) to value-added carbon products such as carbon monoxide (CO) (*1*, *2*). Electrolytic approaches benefit from using water as the reaction medium, as it is a cheap, abundant, and environmentally benign solvent that facilitates proton and electron transfer (*3*, *4*). However, the competitive and often kinetically favored off-pathway reduction of water itself to hydrogen must be avoided. In this context, molecular catalysts for electrochemical CO_2 conversions can be systematically tuned to achieve high activity and selectivity over proton reduction (*5*–*13*), but they typically require organic media to achieve optimal selectivity and/or stability, often to maximize solubility and minimize water- or proton-induced catalyst degradation and/or hydrogen production. In contrast, heterogeneous catalysts are often stable in water, but optimizing their activity through structural changes at a molecular level remains a substantial challenge (*14*–*19*). Against this backdrop, we sought to investigate crystalline porous frameworks—specifically, covalent organic frameworks (COFs) (*20*–*22*)—as tunable materials for electrocatalysis. We reasoned that such materials could potentially combine advantages of both molecular and heterogeneous catalysts: (i) Construction with molecular building blocks would enable precise manipulation of the spatial arrangement of catalytic centers within the predetermined COF structure (*23*); (ii) the frameworks could be expanded and functionalized without changing the underlying topology of the structure (*24*, *25*); and (iii) the conserved pore environment around the active sites within the COF could be tuned electronically and sterically (*26*) while providing ready access for the substrate (*27*–*32*) (Fig. 1). Moreover, these crystalline porous frameworks offer the possibility to perform multivariate synthesis, in which topologically identical and yet functionally modified building blocks can be introduced into the structure. This approach can potentially give rise to materials with emergent properties that are greater than the sum of the individual molecular parts, because one can predictably prepare a topologically ordered framework yet introduce heterogeneity in the number and ratio of functionalities by the choice of building blocks (*33*). Here we show that incorporation of catalytic cobalt porphyrin (*34*) units into COFs, along with multivariate synthesis of frameworks bearing catalytic cobalt and structural copper units, gives highly active, stable, and selective catalysts for electrochemical reduction of carbon dioxide to carbon monoxide in water. A member of the COF series that we studied exhibits a 26-fold increase in activity compared with the parent molecular precursor and, in many respects, outperforms state-of-the-art molecular and solid-state catalysts, with broad opportunities for further improvement through modular synthesis using appropriate combinations of building units. X-ray absorption measurements reveal that the COF framework can directly influence the electronic structure of the catalytic cobalt centers, in a manner akin to redox noninnocent ligand behavior observed in molecular systems (*35*), thereby contributing to the observed gains in reaction selectivity and activity beyond the steric effects of surface area and site isolation.

We focused our initial electrocatalysis studies on COFs, as we sought to exploit the charge-carrier mobility of these materials derived from π conjugation and π-π stacking (*22*, *36*–*38*), as well as the stability from reticular assembly with strong covalent bonds. We synthesized a model framework (COF-366-Co) by the imine condensation of 5,10,15,20-tetrakis(4-aminophenyl)porphinato]cobalt [Co(TAP)] with 1,4-benzenedicarboxaldehyde (BDA) (Fig. 1). The porous COF material was evacuated by activation with supercritical carbon dioxide and heating to 100°C for 18 hours. The retention of cobalt in the coordinating porphyrin units within the framework was confirmed by elemental analysis (supplementary materials section S1.1), thermogravimetric analysis (fig. S1), and

[1]Department of Chemistry, University of California, Berkeley, CA 94720, USA. [2]Chemical Sciences Division, Lawrence Berkeley National Laboratory, Berkeley, CA 94720, USA. [3]Materials Sciences Division, Lawrence Berkeley National Laboratory, Berkeley, CA 94720, USA. [4]School of Physical Science and Technology, ShanghaiTech University, Shanghai, 201210, China. [5]Department of Materials Science and Engineering, University of California, Berkeley, CA 94720, USA. [6]Kavli Energy Nanoscience Institute, Berkeley, CA 94720, USA. [7]King Fahd University of Petroleum and Minerals, Dhahran 34464, Saudi Arabia. [8]Howard Hughes Medical Institute, University of California, Berkeley, CA 94720, USA. [9]Department of Molecular and Cell Biology, University of California, Berkeley, CA 94720, USA.
*These authors contributed equally to this work. **†Corresponding author. E-mail: yaghi@berkeley.edu (O.M.Y.); chrischang@berkeley.edu (C.J.C.)**

Science

A self-interfering clock as a "which path" witness

Yair Margalit, Zhifan Zhou, Shimon Machluf, Daniel Rohrlich, Yonathan Japha and Ron Folman

Science **349** (6253), 1205-1208.
DOI: 10.1126/science.aac6498originally published online August 6, 2015

Interfering with time

The interference pattern arising from light or particles passing through a double slit is a simple experiment that belies the subtleties of interpretation when attempting to describe and understand the effect. For example, determining "which path" the light or particles travel can result in the interference pattern disappearing. Margalit *et al.* present a new take on interferometry using time (see the Perspective by Arndt and Brand). A clock—i.e., the internal state of a cold atom condensate––was coherently split and brought back together to interfere. Making one-half of the clock tick at a different rate resulted in a change in the interference pattern, possibly as a consequence of the time being a "which path" witness.

Science, this issue p. 1205; see also p. 1168

Science (print ISSN 0036-8075; online ISSN 1095-9203) is published by the American Association for the Advancement of Science, 1200 New York Avenue NW, Washington, DC 20005.